Meteor radiant activity mapping using single-station radar observations

J. Jones[1]★ and W. Jones[2]

[1]*Physics and Astronomy Department, University of Western Ontario, London, Ontario N6A 3k7, Canada*
[2]*Materials Research Institute, Sheffield Hallam University, Sheffield S1 1WB*

ABSTRACT

We describe a method for producing high-resolution maps of the radiant distribution of meteor activity over the celestial sphere using single-station radio-meteor observations. The method uses a convolution technique and we show how a suitable convolution function can be chosen to enhance the apparent activity of meteor shower radiants. We apply this method to data produced by the Canadian Meteor Orbit Radar system near London, Ontario and show that the daily motion of the radiant can be measured within a fraction of a degree per day. The system has detected a number of weak showers that have not been previously catalogued. We show how the sensitivity of the system can be improved by combining observations from several days.

Key words: meteors, meteoroids.

1 INTRODUCTION

The details of the evolution of the meteoroid complex are not well understood and their elucidation constitutes an exciting intellectual challenge. The rewards of meeting this challenge successfully not only provide the satisfaction of knowing how the interaction of the various processes involved produce what we observe in the Sky from the Earth, they can but also provide a valuable predictor of potentially hazardous locations and times for space vehicles.

Although valuable measurements can be made using photographic and television techniques, the advantages afforded by a meteor radar are impressive. Able to operate both day and night in almost all weather conditions, meteor radars typically yield many thousands of meteor echoes in a 24-h period with the observational data in a form that is well suited to real-time analysis.

Probably the most important dynamical parameters that can be deduced from observations of a meteor are its speed and its direction, since these determine its orbit. While there are a variety of methods for estimating the meteoroid speed from a single-station meteor radar (Baggaley & Grant 2005), there is as yet no easy method to find the direction of flight of the meteoroid – also known as the radiant – and it is the determination of the radiant that is the focus of this paper. We do have partial knowledge of the radiant if we can determine the direction of the echo, since the specular reflection condition dictates that this is perpendicular to the axis of the meteor train. In this paper, we present a statistical method for recovering the radiant distribution from the meteors observed over a day.

The most ambitious meteor radar systems such as Advanced Meteor Orbit Radar (AMOR; Baggaley et al. 1994) and Canadian Meteor Orbit Radar (CMOR; Jones et al. 2005), which determine the orbital parameters of individual meteoroids, are sophisticated and expensive multistation facilities that require constant maintenance and attention. This paper describes how much simpler single-station meteor radars can be used to monitor the radiant distribution of the incident meteoroids. The technique has been used for the past several years with the CMOR radar and has proved to be very useful for the detection of weak showers as well as being a valuable tool for monitoring the activity of the sporadic meteor sources. CMOR is particularly well suited to this purpose since it is an all-sky system and even in the single-station mode is able to provide unambiguous measurements of the directions of the radar echoes from the meteor trains to better than $1°$, and because it collects several thousand meteor echoes every day, the statistics are very good. In the much more complex multistation mode that combines the measurement of time-delays of echoes from two remote receiving stations together with the determinations of the echo directions, CMOR is presently able to determine the directions of the trajectories of individual meteoroids to a precision of about $2°$ which is limited predominantly by the uncertainties in the measurements of the time-delays rather than the measured echo directions. Indeed, the measurement of the time-delays has proved to be a greater technical challenge than first anticipated and our algorithms for its determination are constantly being improved. System complexity is the price of the trajectory information of individual meteoroids, and for many purposes such detailed information is not required. This paper describes a method of using single-station meteor radar to recover the distribution of meteor radiants over the accessible celestial sphere.

In the following sections, we give the theory of the method and describe how it has evolved since first conceived. We then present examples of how the method performs when applied to observational data collected with the CMOR radar. Finally, we suggest some possible ways in which the technique may be improved and extended.

The method described here is now used extensively for the analysis of CMOR observations and this is intended to serve

★E-mail: jimeteor@uwo.ca

as a comprehensive reference for future studies that will use it.

2 THE METHOD

For more than half a century the radiants of radio meteors have been measured by exploiting the specular reflection condition (Lovell 1954; McKinley 1961). The present method has its roots in the work of Jones (1977) that enabled the distribution of echo directions to be transformed into the distribution of radiant directions using a method based on expansions of the distributions in terms of spherical harmonics. This method proved to be extremely computationally intensive and is not suited to dealing with thousands of echoes. Poole (1997) revisited the spherical harmonic method and replaced the lengthy calculation of the spherical harmonic functions by much faster approximations; nevertheless, it was still not fast enough to deal with thousands of echoes at the resolution required for imaging shower meteor radiant distributions. Poole's modification was, however, adequate for extracting the radiant distributions of sporadic meteors for which high resolution was not required.

Siderov & Kalabanov (2003) have adopted completely different approach known as the 'quasi-tomographic method' which we hope to compare with the present method in a future paper.

To achieve greater computational efficiency, Morton & Jones (1982) adopted the convolution method illustrated in Fig. 1. Unit vector test radiants, T, are systematically chosen over the celestial sphere and the activity of a given radiant is said to be the number of echoes that are perpendicular to T within a specified angle. When T is coincident with the actual radiant, R (also a unit vector), the unit vector echo directions, E, that are perpendicular to R fall on the great circle (GC) within the 'acceptance band' which has some half-width x_0. The half-width of the acceptance band should be about twice the expected radius of the radiant to ensure that the majority of echo points fall within the acceptance band when the trial and mean radiants are coincident. In essence, the procedure is equivalent to convolving the distribution of echo directions with the function, $w(x/x_0)$, where x is just the scalar product $T \cdot E$. Jones and Morton used a 'top-hat' function for $w(x)$ as shown in Fig. 2.

In its basic form, the convolution and spherical harmonic methods share a basic failing: there is an ambiguity in the resultant radiant
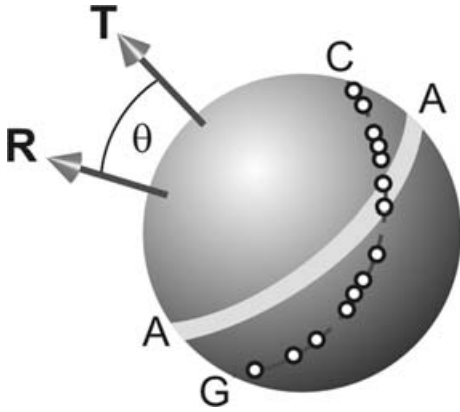

Figure 1. Simple method of recovering radiant distribution. The specular reflection condition causes echoes from meteors approaching from the radiant, R, to produce echoes (small circles) on the GC of the celestial sphere. When the trial radiant T and the actual radiant are coincident, the echoing points fall in the white acceptance band AA and are included. When the trial and actual radiants are not coincident, only those echoing points that fall within the acceptance band are included in the sum.
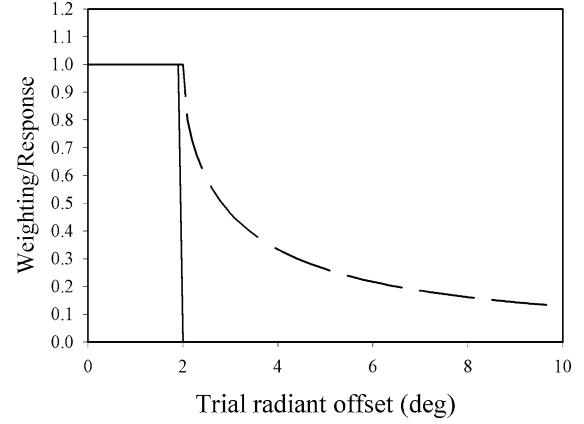

Figure 2. The 'top-hat' acceptance function (solid line) as a function of the trial radiant offset, θ, that is, the angle between the actual (R) and trial (T) radiants. In this case, the weighting function is set to accept all echoes that meet the specular reflection condition within $2°$. The dashed line denotes the response to the top-hat function as a function of the angle between the actual and trial radiants.

directions since the sense of the perpendicular to the plane containing the echo GC is not defined. For the convolution method, this ambiguity is easily resolved if the time of occurrence of a particular echo is available. One merely needs to know if test radiant is above the local horizon when the echo was observed. It is much more awkward to incorporate the time information for the spherical harmonic method.

The response produced with the convolution function of a point radiant at the pole, $r(\theta)$, where θ is the polar angle, is easily calculated using the expression

$$r(\theta) = \int_{\text{GC}} w(\sin(\theta)\sin(\phi))\,d\phi, \qquad (1)$$

where the integral is taken round the echo GC.

The 'top-hat' convolution function is not optimum in that the response from a point radiant has a very diffuse halo. This occurs because even when the test radiant is far from the actual radiant, the echo GC and the acceptance band always intersect with the result that those echoes in the intersection region will be included in the sum. The response function therefore never falls to zero as shown in Fig. 2 and we need to find a better convolution function to minimize this effect. We also note that the sum of echoes, after the simple top-hat filter has been applied, is always positive and can be converted directly into intensity when generating an image of the radiant distribution.

The first improvement is to surround the acceptance band, AA, by a rejection bands, BB, as shown in Fig. 3. Those echo directions falling within the acceptance band are added to the count while those falling within rejection band are subtracted from it. We still get the same echo count as previously if the echo GC falls completely within AA, but the count is attenuated when some of the echo GC falls in the BB region. With the appropriate choice of width for BB, we can ensure that the total count can be made close to zero whenever the echo GC makes an appreciable angle with the acceptance band. A little thought shows that the condition that the tails of the response function vanish is

$$\int_{\text{GC}} w(E \cdot T)\,d\phi \approx 0. \qquad (2)$$
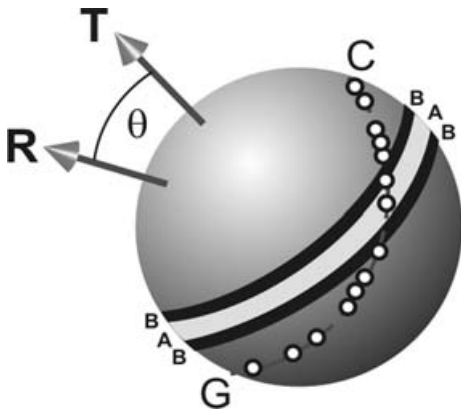
Figure 3. Improved method of recovering radiant distribution. Points falling in the white band, AA, are added to the total while those falling in the black bands, BB, are subtracted from it.

Probably the simplest function to meet this requirement which we will term as the three-band function is

$$w(x) = \begin{cases} +1 & \text{for } |x/x_0| < 1 \\ -1 & \text{for } 1 < |x/x_0| < 2 \\ 0 & \text{for } |x/x_0| \geqslant 2 \end{cases} \quad (3)$$

as shown in Fig. 4, where x is given by

$$x = \sin(\xi) \text{ and } x_0 = \sin(\xi_0), \quad (4)$$

with ξ_0 being the half-width of the acceptance band which has an area equal to that of the total area of the rejection bands. The response function associated with the three-band function shown in Fig. 4 yields a greatly reduced halo at the expense of some overshoot which is the result of the spherical geometry. In contrast to the top-hat filter, the output from the three-band filter can have both negative and positive values because the finite sample size renders it unlikely that the positive and negative contributions will cancel precisely. When producing an image, we regard negative values as non-physical and use only the positive values of the filter output to generate the image.

Fig. 4 represents the ideal case for a very large number of echoes. If only a small number of echoes are associated with a particular radiant, the combination of sharp boundaries between the accept and reject regions of the three-band function and small-sample statistics lead to spurious fluctuations when echo points move from the add
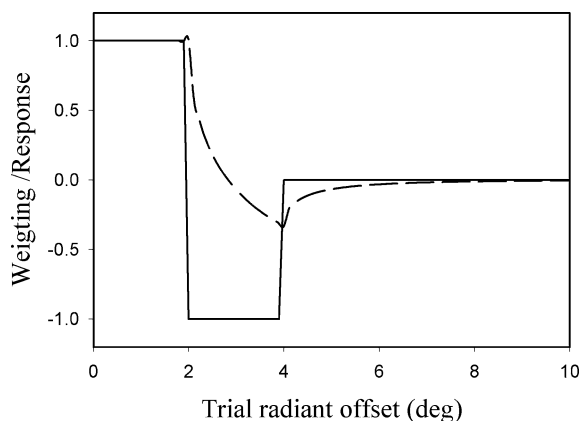

Figure 4. Behaviour of the three-band weighting function with $\xi_0 = 2^\circ.0$. Solid line: weighting function and dashed line: response.
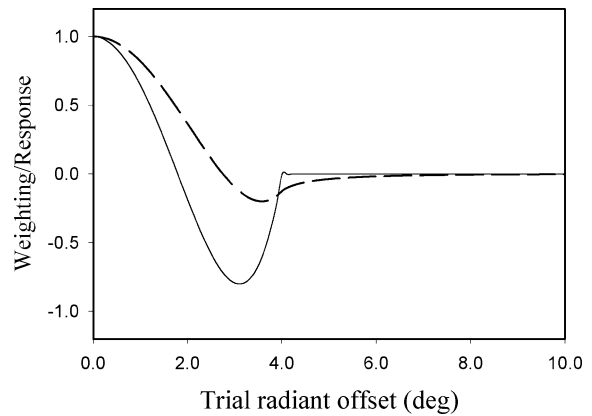

Figure 5. Behaviour of weighting function given by equation (5) with $\xi_0 = 4^\circ.0$. Solid line: weighting function and dashed line: response.

to the subtract regions as the test radiant probes different regions of the celestial sphere that can be regarded as 'noise'. This unwanted contribution to the response can be reduced by use of a convolution function without discontinuities such as that given by

$$w(x) = \begin{cases} 1 - 6\left(\frac{x}{x_0}\right)^2 + 5\left(\frac{x}{x_0}\right)^4 & \text{for } |x| < x_0 \\ 0 & \text{for } |x| \geqslant x_0, \end{cases} \quad (5)$$

where ξ_0 in this case is the half-width of the region that includes both the acceptance and the rejection bands. The function is even as it needs to be and having so few terms and being a polynomial requires a very little computational overhead. The convolution function and its associated response are shown in Fig. 5.

How do we choose a value for ξ_0? In practice, the shower radiants are not points on the celestial sphere but have a finite width as a result of the processes by which they were generated as well as gravitational perturbations by the planets and radiation forces. From the analysis of high-precision photographic studies of shower meteors, Whipple & Wright (1954) found that the intrinsic radiant scatter is seldom greater than 1°. Brown (1999) has shown that the scatter due to gravitational perturbations dominates after a few revolutions of the parent comet so that we might expect the intrinsic scatter to be substantially independent of mass. There is also a measurement error, which with a well-designed interferometer as is used by CMOR (Jones, Webster & Hocking 1998) can be less than 1°. The composite apparent radiant spread is typically of the order of 1° and this is confirmed by observations using CMOR. We consider a value of 4° for ξ_0 (corresponding to a half-width of the acceptance band of about 2°) to be a good compromise between resolution and the strength of the response. For a point radiant, this value of ξ_0 produces an image with half-width of about $1^\circ.8$ as shown in Fig. 5.

3 RADIANT AREA

Since the radiants have a small but appreciable width, we need to consider how the intensity and width of the image depends on the diffuseness of the radiant. In Fig. 6, we show how the maximum response of the convolution filter varies as a function of diffuseness of the radiant. It is evident that our convolution function discriminates against diffuse radiants. Indeed, it is easy to see that the response of the filter in the limiting case of an isotropic distribution of radiants is zero, since the areas of the acceptance and rejection bands are equal. On the other hand, the filter excels in imaging small, discrete
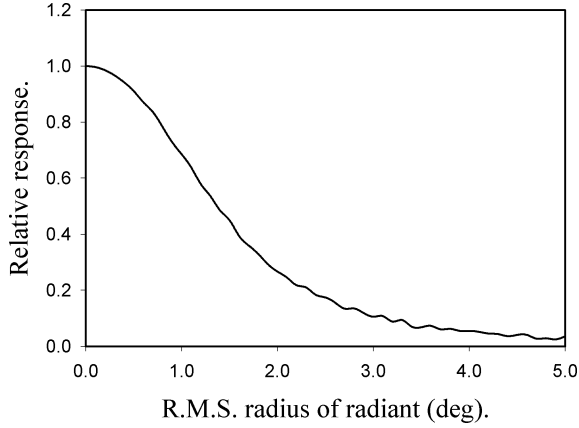
Figure 6. Relative response of weighting function given by equation (5) with $\xi_0 = 4°0$ as a function of the diffuseness of the radiant area.
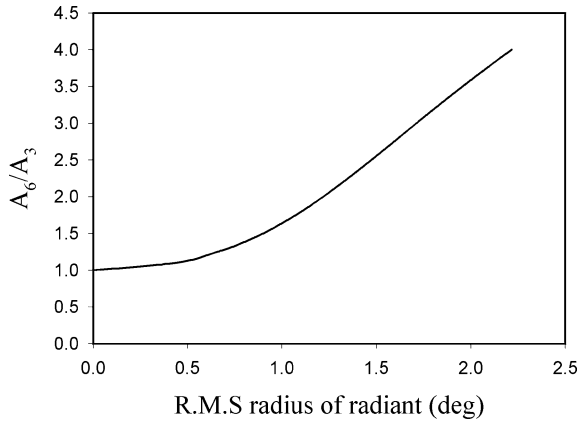

Figure 7. Ratio of responses with $\xi_0 = 6°$ and $3°$ as function of effective radius of radiant.

radiants and yields its greatest response for point-source radiants. This kind of convolution function is therefore ideal for imaging the radiants of meteor showers while at the same time reducing the contribution of wide sources of meteor activity such as the Helion, Antihelion, Apex and Toroidal sporadic sources which have radii of the order of $15°$–$20°$ (Jones & Brown 1993).

Since the response is determined by both the diffuseness of the radiant and the width of the convolution function, we have a method of estimating the radiant diffuseness: we need merely to determine the apparent activity, A, of a given shower for two different well-chosen values of ξ_0. In practice, we find that $\xi_0 = 6°$ and $3°$ provide good results. With these values, we find that the ratio $A_6 : A_3$ varies with the effective radius of the radiant (intrinsic radius plus measurement error) as shown in Fig. 7.

4 GENERATION OF THE IMAGE OF THE RADIANT DISTRIBUTION

Maps of the radiant activity are easily generated using the equation

$$A_j = \sum_i w(\mathbf{T}_j \cdot \mathbf{E}_i) F(\mathbf{T}_j, \mathbf{E}_i), \qquad (6)$$

where A_j is the strength of the radiant in the jth direction and the summation is taken over all the observed meteor echoes and F is a

function with a value of unity if $\mathbf{T}_j$ is above the local horizon at the time of occurrence of the ith echo and zero otherwise.

It is important to distinguish between the notions of an image of the radiant activity and a map of the radiant activity. Because the actual radiant activity at any point on the celestial sphere can never be negative but the apparent radiant activity (the radiant map) calculated from equations (5) and (6) can have negative values, we have to decide how to deal with this. The simplest approach is to convert all negative values to zero when generating the image of the radiant activity but we must not discard the negative values altogether. The negative values arise because we are dealing with finite sample sizes and incomplete cancellations are apt to occur in regions where the radiant activity is low and this is manifest as a 'noise' that can render weak radiants difficult to discern. The radiant maps contain more information than the images of the radiant activity, whereas the latter can always be generated from the former, but the converse is not true. In practice, we store only the radiant map data and generate the images from it as needed.

It is convenient to display the images of the radiant activity using the Mollweide (Babinet 1859) equal-area projection because of the ease of transformation from right ascension (RA) and declination (Dec.) into the rectangular coordinates of the projection and vice versa. Because we expect the effective radiant radius to be of the order of $1°$ as shown in Section 3, we choose to scan the Mollweide projection using a rectangular 201×101 grid of points which provides a spacing of sample points of approximately $1°8$. The final plots were then expanded to 801×401 using bicubic spline interpolation. This appears to be the optimum procedure since the use of a finer sampling grid does not produce a map of finer resolution but merely takes more time to compute. We find that it takes about 15–20 s on a 1-GHz PC to generate an activity map from the observations of a single day.

5 APPLICATION TO OBSERVATIONAL DATA

In this section, we have applied our method of radiant imaging to observational data from the CMOR system operating in single-station mode at 29 MHz. For the CMOR system, described in detail by Jones et al. (2005), the peak pulse power is 6 kW; the pulse length is 75 s with pulse repetition frequency of 532 Hz; the gain of the transmitting antenna is 7.6 dBi; the echo directions are determined using the five-element interferometer described by Jones et al. (1998) with the gain of each receiver antenna being 6.3 dBi giving a limiting magnitude for the system close to $+8.9$.

In Fig. 8, we present an example of an image using the 'top-hat' filter of the radiant distribution (in RA, Dec. coordinates) from the distribution of radio-meteor echo direction distributions obtained with CMOR in 2003 January 2. Although the region of strong activity due to the Quadrantid meteor shower (RA $= 231°$ and Dec. $= 48°$) is clearly visible, the image is far from satisfactory. But in spite of its imperfections, Poole & Roux (1989) have used this method to provide useful measurements of the radiants in the Southern hemisphere.

Fig. 9 shows the image of the radiant distribution produced by applying the filter described by equation (3) to the same observational data that were used to produce Fig. 8. The improvement resulting from the use of the polynomial convolution function is very evident. In addition to the early activity of the Quadrantid shower at RA $= 231°$ and Dec. $= 48°$, a weak shower is also clearly visible at RA $= 149°$ and Dec. $= 26°$ that does not appear in catalogues of minor meteor showers.
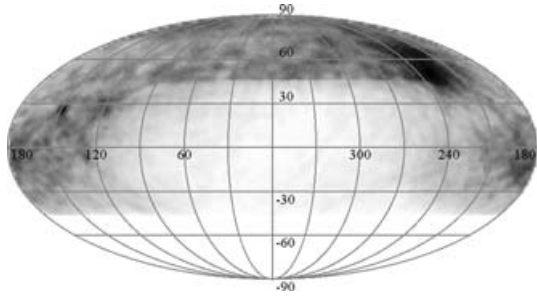
Figure 8. Image of radiant distribution in 2002 January 2 obtained with CMOR data using top-hat convolution function. The horizontal scale is RA and the vertical scale is Dec. Note the severe effect of the diffuse halo associated with this filter that appears round the centres of activity. The image is a negative one with increasing darkness corresponding to increasing strength of the radiant activity.
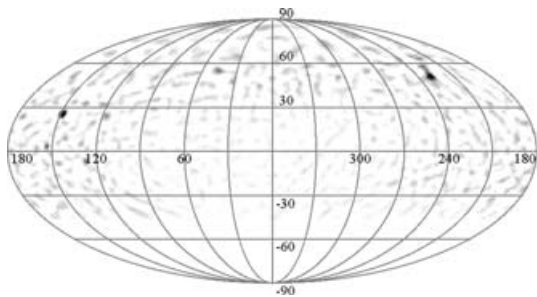

Figure 9. Image of radiant distribution in 2002 January 2 obtained with CMOR data using the convolution function given by equation (5) with $\xi_0 = 4°$.

In Section 2, we discussed how the value of ξ_0 was initially chosen on the basis of photographic determinations of the radiant area. We wish to know whether the apparent radiant radii are close to the photographic values or they are dominated by uncertainties in the determination of the echo directions. In Section 3, we proposed a simple procedure for estimating the radiant scatter from measurements of the apparent strength of shower radiants made of different settings of the resolution parameter ξ_0, and the radiant scatter for several showers determined in this way listed in Table 1 shows that in fact the measured radiant scatter is dominated by measurement errors in the echo directions. We therefore adopted $\xi_0 = 4°$ as an acceptable compromise between resolution and apparent radiant activity. With this value, the apparent strength of a radiant of intrinsic width of $1°$ is about 70 per cent of its true value. The corresponding factors for radiants of other degrees of diffuseness can be read from Fig. 6.

6 OBSERVATIONS OF A METEOR SHOWER

We now apply the method to observations made by CMOR in the interval 2003 October 15–31 during the Orionid shower for the purpose of demonstrating the consistency of the results, it yields. The Orionid shower is moderately active – typically with zenithal rates of about 20 per cent of the Geminid and Perseid showers. In Fig. 10, we show the meteor count for the observed Orionid radiant as a function of solar longitude. The shape of the shower activity profile from the CMOR observations is similar to that obtained from visual observation described by Rendtel, Arlt & McBeath (1995).

Table 1. Estimated radiant scatter (rms) for several meteor showers as determined from the ratio of the apparent strength of the radiants with $\xi_0 = 6°$ and $3°$. The photographic data are taken from Whipple & Wright (1954) and Jacchia & Whipple (1961).

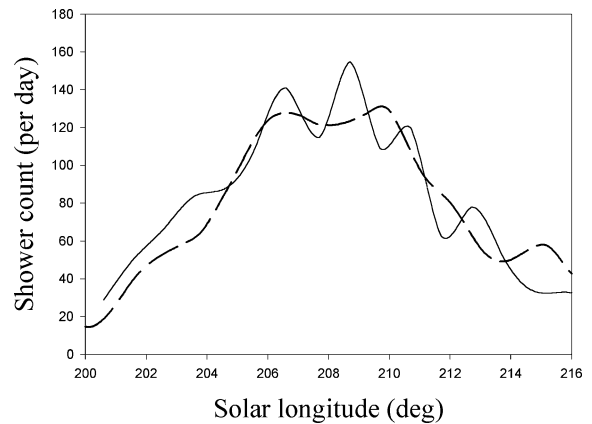| Shower	Present work (°)	Photographic (°)
Quadrantids	1.6	1.9
Arietids	1.4	–
S δ Aquarids	1.1	0.80
Perseids	1.1	0.68
Sextantids	1.4	–
Orionids	1.0	0.38
Monocerotids	1.1	–
Geminids	1.2	0.22

Figure 10. Measured activity of the Orionid shower for 2003. Solid line: present method applied to CMOR single-station radar observations and dashed line: visual observations by Rendtel et al. (1995).
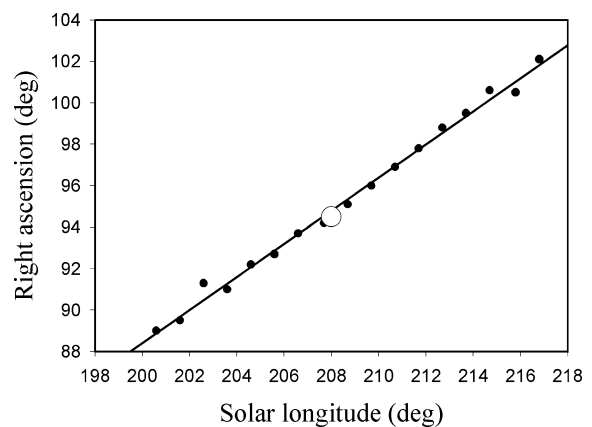

Figure 11. Measured RA of the Orionid shower for 2003. The large circle represents the nominal RA at the shower maximum given by Rendtel et al. (1995).

Although the theory of the daily motion of the radiant is beyond the scope of the present paper, observations of this motion provide a good indication of the errors in the determinations of the radiant position. Figs 11 and 12 show plots of the variation of the RA and Dec. of the radiant (uncorrected for zenithal attraction and diurnal variation) with solar longitude and it is clear that even close to the beginning and end of the shower where the echo count is low, the
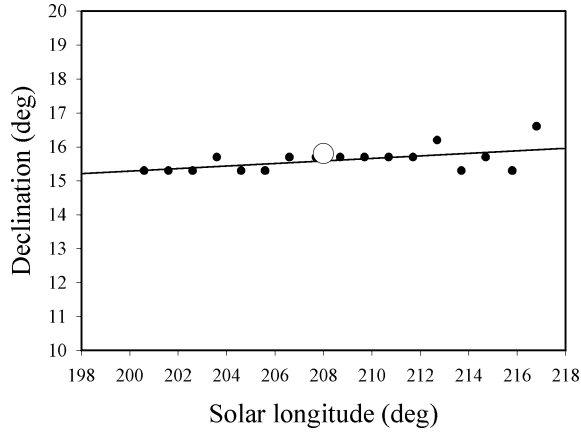
Figure 12. Measured Dec. of the Orionid shower for 2003. The large circle represents the nominal Dec. at the shower maximum given by Rendtel et al. (1995).

Table 2. Mean position of the 2003 Orionid radiant for $\lambda_\odot = 208°$.

	Present work	Cook (1973)	Rendtel et al. (1995)
RA (observed)	$94°0 \pm 0°6$	–	–
Dec. (observed)	$15°1 \pm 0°6$	–	–
RA (corrected)	$94°1 \pm 0°6$	$94°5$	$95°$
Dec. (corrected)	$15°3 \pm 0°6$	$15°8$	$16°$

Table 3. Mean daily motion of the 2003 Orionid radiant.

	Present work	Cook (1973)	Rendtel et al. (1995)
RA	$0°801$	$1°23$	$0°65$
Dec.	$0°04$	$0°13$	$0°11$

accuracy of the determination of the radiant position is good. Table 2 gives the measured and corrected values of the radiant position and Table 3 gives its daily motion. The radiant position obtained here is in excellent agreement with that based on the visual and photographic studies. The agreement for the daily motion of the radiant is much poorer, possibly the result of the smaller numbers of Cook's photographic observations. Since no uncertainties are provided with the radiant positions of either Cook or Rendtel et al., the discrepancies may not be significant.

7 INTEGRATION OF DATA SETS

Weak showers are often difficult to detect in the observations of a single day as shown in Fig. 13. Although numerical experiments have confirmed that the method does not generate bogus radiants, the noise background resulting from the limited number of echoes can obscure weak centres of activity. By combining several days worth of observations, we can enhance persistent features. For example, we can combine the images from the separate days as shown in Fig. 14 but, as discussed in Section 4, this results in a very obvious background caused by the non-cancellation of the noise component. A better solution is to sum the radiant activity maps prior to their conversion into images, since these still include the negative values that provide the possibility of cancellation of the noise. The result of this procedure is presented in Fig. 15 and it is evident that there are
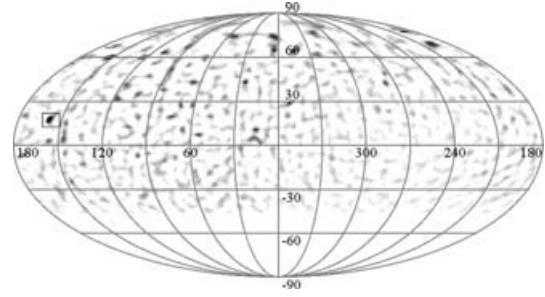

Figure 13. Example of a radiant map from a day (2003 September 22) when the meteor shower activity was relatively quiet. Note that the region of activity marked by the rectangular box is not more conspicuous than the several other regions of enhanced activity and it is not clear from the observations of a single day, whether any of these areas are genuine weak showers or the result of random fluctuations due to low-count statistics.
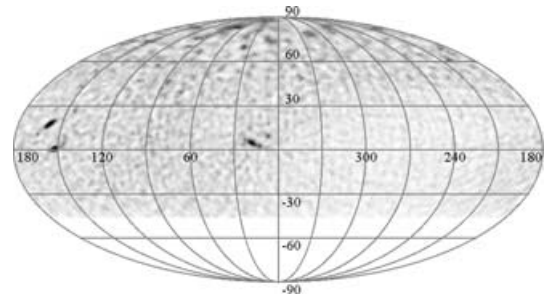

Figure 14. Image of the radiant distribution calculated by combining images generated from CMOR data in the period 2003 September 15–30. Note that even though the process of combining images emphasizes the persistent features, it raises the overall background arising from low-count statistical fluctuations.
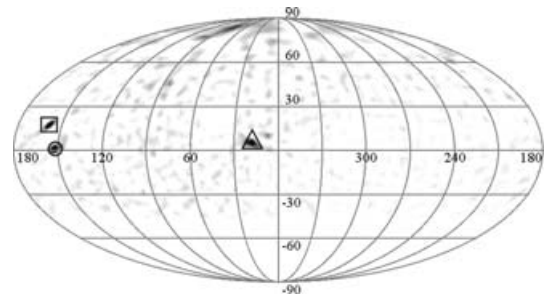

Figure 15. Image of the radiant distribution calculated by combining activity maps generated from CMOR data in the period 2003 September 15–30. By combining radiant maps rather than radiant images, we make the persistent features more prominent while reducing the background arising from low-count statistical fluctuations.

at least three weak but active showers present, marked by a circle – the Sextantids at RA = $152°5$, Dec. = $0°5$, a rectangle at RA = $159°0$, Dec. = $18°4$ and a triangle at RA = $19°4$, Dec. = $5°0$; the two latter showers do not appear in the catalogues of either Cook (1973) or Sekanina (1976).

8 DISCUSSION

Single-station meteor radar systems are both less complex and less expensive than multistation orbital radars. They also register

more meteor echoes since the requirement that the meteor must be observed at least three stations for a multistation system severely reduces the number of usable echoes. In short, the price paid for simpler hardware and software is that the directional information for individual meteor trains is limited to a plane perpendicular to the echo direction. Nevertheless, if we are content to use statistical methods, we can still retrieve the radiant distribution of meteoroids. For many purposes that do not require information about individual trains, the single-station is superior to the multistation technique.

The method described here is especially well suited to meteor shower studies in that the convolution filter used is optimized for shower radiants that are collimated within a degree or so. It discriminates against more diffuse radiants though it is possible to optimize the filter for much broader sources such as the sporadic Helion and Antihelion sources. We plan to describe such a filter in a future paper.

The method is also extremely sensitive. Typically, CMOR yields echoes from 7000 meteor trains per day and it is possible to measure accurately radiant positions of weak meteor showers with as few as 30 meteors per day. If the shower persists for several days it is often possible to make accurate determinations of the radiant motion. Because the system is so sensitive to shower meteors, it detects many weak showers that have not been previously recognized. On initial inspection, it is sometimes uncertain whether these possible showers are real or the result of the small-sample sizes. By combining observations from several days and years, we can render the persistent features more prominent. By using single-station measurements of the meteoroid speeds together with the radiant determinations, we can determine the mean orbital elements of these weak streams and future papers will describe the results of such minor stream searches in detail.

It has been suggested that the sporadic meteoroid background is a composite of ancient meteor streams that have been dispersed as a result of planetary gravitational perturbations and radiation forces. The present method provides a means of discerning fine structure of the sporadic background and hence a means of testing that suggestion.

REFERENCES

Babinet J., 1859, Geographic Nouvelle: Mappemondes et Cartes, System Homalographiques. Ernest Bourdin, Paris

Baggaley W. J., Bennett R. G. T., Steel D. I., Taylor A. D., 1994, QJRAS, 35, 293

Baggaley W. J., Grant J., 2005, Earth, Moon and Planets. In press

Brown P., 1999, PhD thesis, Univ. Western Ontario

Cook A. F., 1973, in Hemenway C. L., Millman P. M., Cook A. F., eds, Evolutionary and Physical Properties of Meteoroids. NASA SP-319, Washington, D.C., p. 183

Jacchia L. G., Whipple F. L., 1961, Smithson. Contrib. Astrophys., 4, 97

Jones J., 1977, Bull. Astron. Inst. Czechosl., 28, 272

Jones J., Brown P., 1993, MNRAS, 265, 524

Jones J., Webster A. R., Hocking W. K., 1998. Radio Sci., 33, 55

Jones J., Brown P., Ellis K. J., Webster A. R., Campbell-Brown M., Krzemenski Z., Weryk R. J., 2005, Planet. Space Sci., 53, 413

Lovell A. C. B., 1954, Meteor Astronomy. Oxford University Press, Oxford

McKinley D. W. R., 1961, Meteor Science and Engineering. McGraw-Hill, New York

Morton J. D., Jones J., 1982, MNRAS, 198, 737

Poole L. M. G., 1997, MNRAS, 290, 245

Poole L. M. G., Roux D. G., 1989, MNRAS, 236, 645

Rendtel J., Arlt R., McBeath A., 1995. Handbook for Visual Observers. International Meteor Organization, Potsdam

Sekanina Z., 1976, Icarus, 27, 265

Siderov V. V., Kalabanov S. A., 2003, Solar Syst. Res., 37, 145

Whipple F. L., Wright F. W., 1954, MNRAS, 114, 229

This paper has been typeset from a TEX/LATEX file prepared by the author.